ELSEVIER

Solid State Ionics 135 (2000) 181–191

SOLID STATE IONICS

www.elsevier.com/locate/ssi

The crystal structural evolution of nano-Si anode caused by lithium insertion and extraction at room temperature

Hong Li[a], Xuejie Huang[a], Liquan Chen[a,*], Guangwen Zhou[b], Ze Zhang[b], Dapeng Yu[c], Yu Jun Mo[d], Ning Pei[d]

[a]*Lab. for Solid State Ionics, Institute of Physics, Chinese Academy of Sciences, Beijing 100080, China*
[b]*Beijing Laboratory of Electron Microscopy, Center for Condensed Matter Physics, Chinese Academy of Sciences, Beijing 100080, China*
[c]*Department of Physics, National Key Laboratory of Mesoscopic Physics, Peking University, Beijing 100871, China*
[d]*Department of Physics, Henan University, Kaifeng 475001, China*

Abstract

The crystal structure and morphology of nanosized Si particles and wires after Li-insertion/extraction electrochemically have been studied by ex-situ XRD, Raman spectroscopy and electronic microscopy. It is confirmed that the insertion of lithium ions at room temperature destroys the crystal structure of Si gradually and leads to the formation of metastable amorphous Li–Si alloy. Furthermore, local ordered structure of Si can be restored after the partial extraction of lithium ions, which indicates the extraction of lithium ions promoting the recrystallization of amorphous Li-inserted Si. It was also observed that nanosized Si particles and wires were merged together after the insertion/extraction of lithium ions.

Keywords: Nanosized Si; Lithium ion battery; Anode; Electrochemical insertion; Electron microscopy; Raman spectroscopy

1. Introduction

It has been reported that a large amount of lithium ions can be inserted into nanosized silicon by an electrochemical method at room temperature [1]. Due to its high reversible capacity and better cyclic performance, nanosized Si may be used as a novel anode active material for lithium ion batteries. It has been suggested that the crystal structure of Si should change with increasing dose of inserted lithium ions.

Electrochemical alloying reaction of lithium with metals has been widely studied since the 1970s [2–8]. Previous studies revealed that Li can form various compounds with Si at elevated temperature, such as $Li_{12}Si_7$, $Li_{13}Si_4$, Li_7Si_3 and $Li_{22}Si_5$ [5,8]. Recently, the structure variation of nanosized Si particles (SiNPs) at heavy Li-insertion state ($\sim Li_4Si$) and partial Li-extraction state at room temperature has been investigated by us using selected area electron diffraction (SAED) [9]. SAED for SiNPs in the Li-insertion state showed a dispersed-ring pattern. It indicates that the crystal structure of Si was destroyed due to the insertion of a large amount of lithium ions leading to the formation of an

*Corresponding author. Tel.: +86-10-82649046; fax: +86-10-82649050.

E-mail address: lqchen@aphy02.iphy.ac.cn (L. Chen).

0167-2738/00/$ – see front matter
PII: S0167-2738(00)00362-3

amorphous structure. SiNPs in partial the Li-extraction state showed a three-order ring pattern. The interplane spaces of the first, second and third order rings are 0.198, 0.146 and 0.118 nm, respectively. It may be related to new short-range ordered structures. However, the microstructure of Li-inserted nanosized Si and the evolution process of Si from crystal to amorphous structure are not very clear at that time.

In this paper, the crystal structural evolution of Si including SiNPs and Si nanowires (SiNWs) has been studied in more detail by using further high-resolution transition electron microscopy (HRTEM) combined with Raman spectroscopy. The morphology of SiNPs and SiNWs after the insertion/extraction of lithium ions has been investigated by scanning electron microscopy (SEM) and TEM.

2. Experimental

Two types of nanosized Si powder were used in this work. One is the ball-shape SiNPs, another is the wire-like SiNWs. Pure SiNPs powder was prepared by laser-induced silane gas reaction [10]. The average size of the Si particles are 80 nm, with a 20 nm distribution measured by a Zetasizer 3000 particle size analytical instrument. SiNWs with a uniform diameter distribution and high purity was synthesized by laser ablation [11,12]. The average diameter of the SiNWs is about 15 nm and the length varies from a few tens to hundreds of micrometers. Each SiNWs has a crystalline core and a thin surface layer of amorphous silicon oxide (about 2 nm) [13].

The SiNPs and SiNWs samples at various lithium insertion/extraction states for TEM and SAED observation were obtained by galvanostatic discharging and charging a typical two-electrode cell to a different voltage [14]. The cell was composed of a metal lithium foil as a counter electrode, 1 M $LiPF_6$ in a 1:1 v/v mixture of ethylene carbonate (EC) and diethyl carbonate (DEC) as electrolyte, Celegard® 2300 as separator and nano-Si as a working electrode. The Nano-Si electrode was prepared by coating the binder-free slurry of SiNPs or SiNWs powder and cyclopentanone directly onto a surface-rough copper foil (0.018 mm in thickness, CARL Schlenk AG, German). The film was dried at 80°C for 8 h under vacuum, compressed under 1×10^6 Pa between two stainless steel plates and cut into pieces with area of 0.8 cm^2 as SiNPs or SiNWs electrodes. All cells were assembled and de-assembled in an argon-filled glove box.

The SiNPs and SiNWs electrode films for TEM observation were taken out from the cells after electrochemical treatments. The sample powder was scratched from the Cu substrate and sealed in a glass tube containing anhydrous benzene in the glove box. After ultrasonic treatment, a droplet of benzene containing dispersed nano-Si particles was placed on a copper grid covered with amorphous carbon film. The Cu grid was sealed in a glass tube and taken out from the glove box. Finally, the Cu grid was transferred into the vacuum chamber of the electron microscope within 30 s. A JEOL –2010 transition electron microscope operating at 200 kV was used to investigate the microstructure of SiNWs.

The morphology of SiNPs was observed by a Hitachi S-4200 scanning electron microscope. The discharged or charged electrode films were taken out from the cells and pasted directly onto a special shelf for SEM in the glove box, then sealed in a glass bottle. During the transfer of the sample shelf from the bottle into the vacuum chamber of the electron microscope, high pure argon gas flow was blown onto the surface of the shelf continuously to minimize the influence of moisture. The whole transfer process was finished within several seconds.

The ex-situ Raman spectra were recorded by a Spex 1403 spectrophotometer with a 488.0 nm Ar-ion excitation line. A specially-designed optical cell was used. It has a quartz window and is vacuum-tight in order to avoid the interference of moisture during the test. The electrode films at different discharged states were placed into the Raman cells in the glove box before the Raman test.

3. Results and discussion

3.1. Ex-situ Raman spectra of SiNPs and SiNWs at different discharged states

Ex-situ Raman spectra of the SiNPs electrode at four Li-insertion levels are shown in Fig. 1. At the lighter Li-insertion level, the Raman peak of c-Si at 518 cm^{-1} can be observed in spectra A and B,

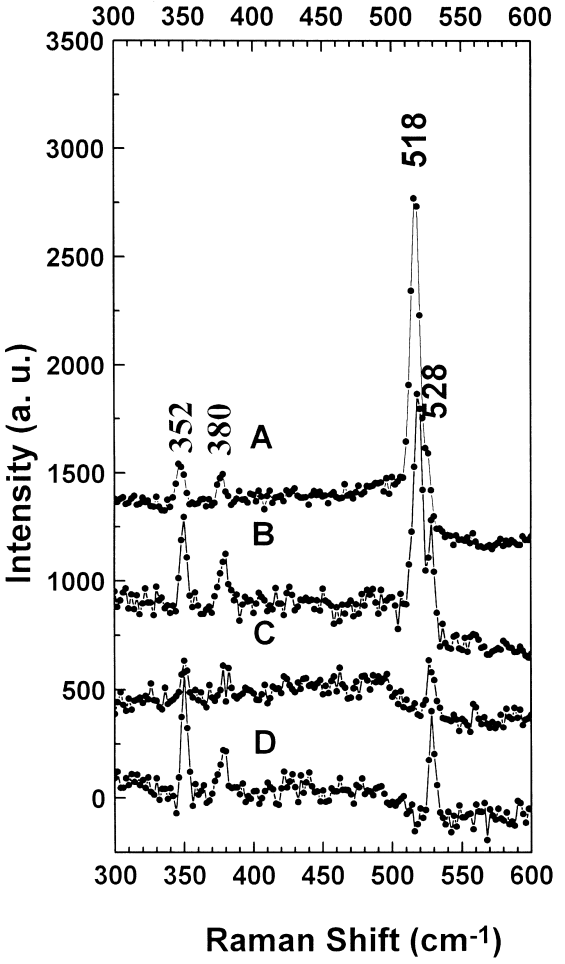

Fig. 1. Raman spectra of the SiNPs electrodes at different discharged states in a lithium cell: SiNPs/1 M $LiPF_6$, EC-DEC (1:1 in v/v)/Li. The SiNPs electrodes were prepared by pasting the slurry of SiNPs powder and cyclopentane onto the surface-rough Cu substrate without any additives. (A) Discharged to 0.6 V, then potentiostat at 0.6 V for 24 h; (B) discharged to 0.4 V, then potentiostat at 0.4 V for 24 h; (C) discharged to 0.0 V, then short-circuit for 24 h; (D) charged to 2.0 V, then potentiostat at 2.0 V for 24 h. The discharge and charge curve are referenced in [1] and [14].

besides three plasma lines related to 488.0 nm excitation. In addition, an amorphous-like component around 480 cm^{-1} seems more significant in spectrum B than that in spectrum A. From the Raman spectra of hydrogenerated amorphous silicon and ion implanted Si, an amorphous component has also been observed [15–17]. This amorphous component results from the disordered silicon structure.

At the heavy Li-insertion level as shown in spectrum C, the peak related to crystalline silicon disappears completely and only a broad peak centered around 480 cm^{-1} can be observed. It indicates that the diamond structure of crystalline silicon has transformed into an amorphous structure. After Li ions were partly extracted from the Li-inserted SiNPs, the peak of c-Si was not recovered as shown in spectrum D. The amorphous component can still be recognized in both spectra C and D.

Fig. 2 shows the Raman spectra of SiNWs at the original state and three Li-inserted states. A peak centered around 516 cm^{-1} corresponding to c-Si can be observed in spectrum A. The shift and broadening of the peak is a typical characteristic of SiNWs caused by quantum confinement effect [18]. At the rather lighter Li-inserted state, the component of c-Si nearly disappeared and an obvious amorphous component was presented as shown in spectrum B. At the heavy Li-insertion state and partly Li-extracted state, the Raman spectra of SiNWs were similar with those of SiNPs. Only the amorphous component can be recognized.

All of the results mentioned above suggest that the insertion of Li ions into the nanosized Si at room temperature leads to the destruction of the crystal structure. As a result, an amorphous Li–Si alloy was formed. It is different from the electrochemical alloy reaction of lithium with Sn, Sb, SnSb alloy at room temperature. Courtney and Dahn have observed the reaction products of SnO with lithium at room temperature by in-situ XRD [19]. The broad peaks presented in the XRD patterns confirm the co-existence of several Li–Sn alloy phases. The present authors observed directly the crystalline stripes of nanosized Li–Sn alloy products by using HRTEM [20]. More recently, we have studied the reaction products of pure Sb and SnSb alloy with lithium at room temperature by ex-situ XRD. The peaks of Li_3Sb or Li_xSn can be recognized [21]. These results confirm that Sn and Sb can react with lithium ions to form crystal Li–M alloys at room temperature instead of amorphous products.

In fact, in most of the cases mentioned above, the XRD peaks related to Li–M alloys are rather broad. It means that these alloys are not long-range ordered

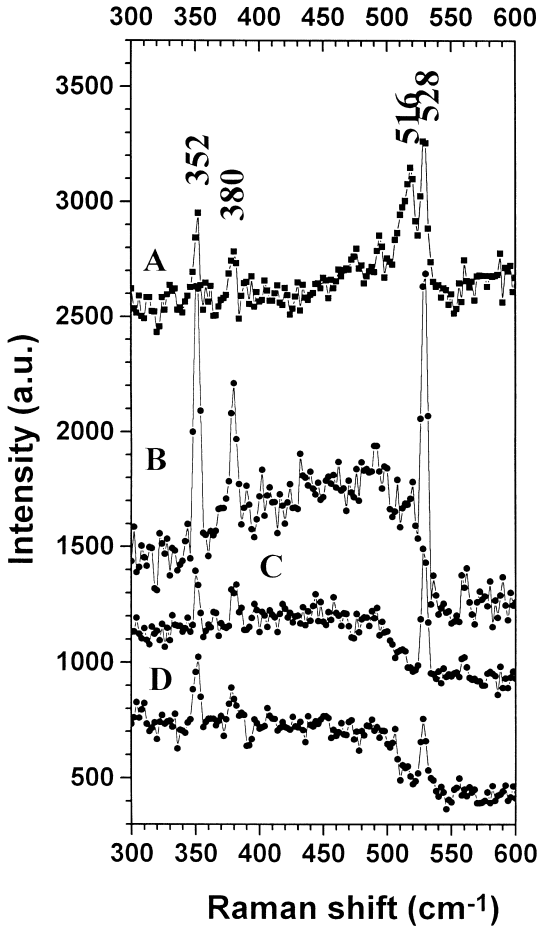

Fig. 2. Raman spectra of SiNWs electrodes at different discharged states in a lithium cell: SiNWs/1 M $LiPF_6$, EC-DEC (1:1 in v/v)/Li. The SiNPs electrode were prepared by pasting the slurry of sponge-like SiNWs powder and cyclopentane onto the surface-rough Cu substrate without any additives. (A) Original SiNWs electrode, (B)–(D) same as Fig. 1(B)–(D).

structures. As suggested by Courtney et al., the low diffusion rate of lithium in the Li–Sn alloy phases at room temperature restrains the formation of the long-range ordered structure [19].

It is reasonable to assume that the insertion of lithium ions destroys the bonds among Si atoms. As a result, a large amount of lithium ions bond with silicon atoms. Each silicon atom may be surrounded by several lithium atoms, especially at the heavy Li-insertion level. Consequently, the ordered sites of Si atoms in the lattice are disturbed and the crystal structure of silicon is destroyed. Thus, the peak representing the lattice vibration mode of bulk silicon disappears in the Raman spectrum. It is also understandable that lithium ions inserted in silicon can not move fast enough to form the ordered Li–Si alloy at room temperature.

3.2. Ex-situ Raman spectra of Li-inserted SiNPs and SiNWs after annealing at 400°C

Since the crystalline Li–Si alloy can be formed at elevated temperature, the amorphous Li–Si alloy formed at room temperature should be considered as a metastable phase and may be transformed into crystalline structure. A vacuum annealing experiment has been performed at 400°C for 5 h. Fig. 3 compares the Raman spectra of Li-inserted SiNPs before and after annealing treatment. Two obvious broad peaks around 520 and 489 cm^{-1} can be observed. Although the influence of lithium bonding with silicon atoms on the Raman spectrum of Si is not clear, a more ordered structure should be expected after the annealing treatment as shown in Fig. 3(B). A similar result was observed in the Raman spectra of Li-inserted SiNWs as shown in Fig. 4(B). The appearance of the peak at 520 cm^{-1} in Figs. 3(B) and 4(B) indicates the existence of c-Si. A possible reason may be that part of the lithium atoms volatilize from the Li-inserted SiNPs during annealing and lead to the restoration of the crystal silicon structure. However, it seems more reasonable that the lithium ions and silicon atoms can move fast enough to occupy more regular sites at elevated temperature and the amorphous Li–Si alloy transforms into the ordered structure. Some more work should be done to make a definite conclusion.

3.3. HRTEM of SiNWs at different Li-insertion levels

The previous SAED patterns of SiNPs at the heavy Li-insertion state and partly extracted state did not provide detailed information about the microstructure of Li-inserted Si [9]. At that time, clear lattice images of SiNPs could not obtained due to its large particle size for HRTEM observation. The formation mechanism of the amorphous Li–Si alloy was not very clear. We had supposed that several

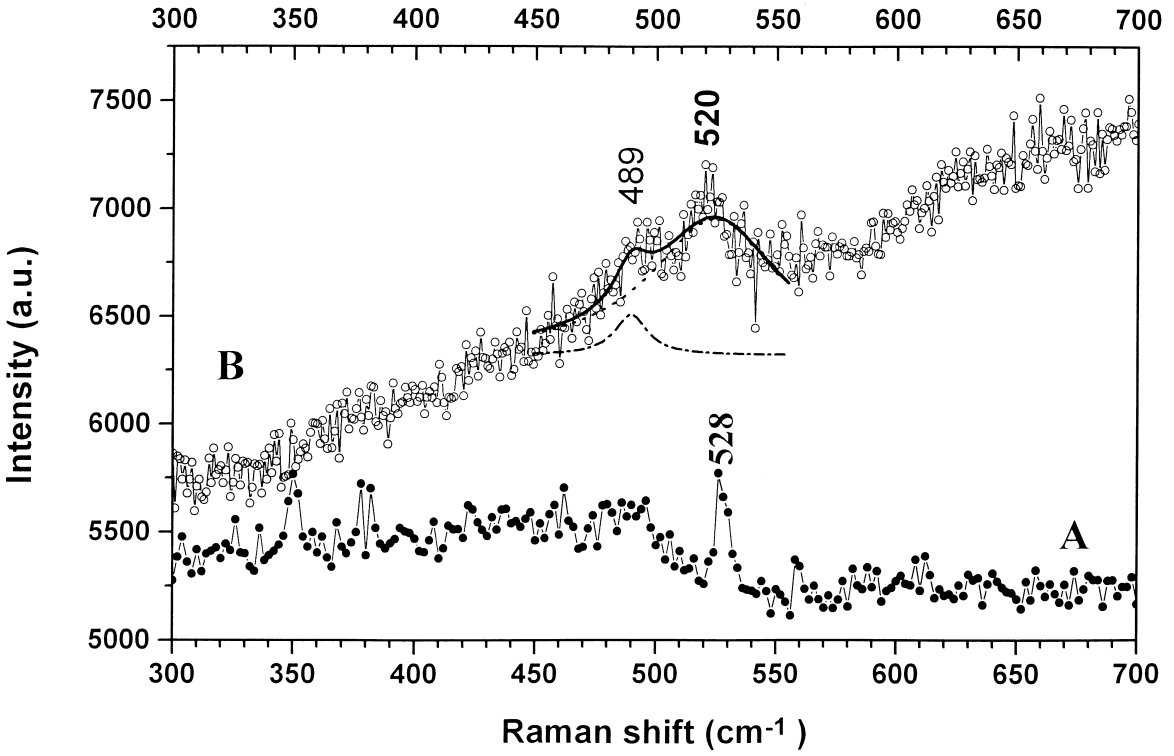

Fig. 3. Raman spectra of Li-inserted SiNPs electrodes after annealing treatment. (A) The same as that in Fig. 1(C); (B) after step (A), then vacuum-annealing at 400°C for 5 h. Dot line and solid line are fitting curves.

intermediate phases may be occurring with increasing dose of inserted lithium [9].

The microstructure of pure SiNWs has been studied by Yu and Lieber. The lattice images of SiNWs were observed clearly using HRTEM [11–13]. Therefore, we used SiNWs as anode active materials to investigate the crystal structure of SiNWs after electrochemical insertion.

Fig. 5(A)–(E) compares the HRTEM images of SiNWs before and after Li-insertion. The image of a single SiNW is shown in Fig. 5(A) in which almost perfect (111) lattice fringes can be seen in the core region. A thin amorphous layer is also observed on the surface of the SiNW. It is composed of silicon oxide [11]. The thickness of the surface oxide layer of each SiNW is close to 2 nm. In fact, in most of the original SiNWs sample, abundant defaults also coexist, such as microtwins, stacking faults and low-angle grain boundaries.

Fig. 5(B) shows the image of SiNWs at the shallow Li-insertion level. The crystalline Si core and amorphous regions can be distinguished clearly from Fig. 5(B). The interplanar spacing for most crystal stripes is 0.31 nm corresponding to the {111} plane of silicon. Thus, these crystal regions can be regarded as the unreacted part with lithium. It can be seen that the amorphous region denoted by black arrows develops from the surface into the core of SiNWs. Due to the inhomogeneity of both electrical contact and the concentration distribution of lithium ions, the width of the amorphous regions is different. A few of the amorphous regions were also found within the crystalline matrix. This may be caused by the penetration of lithium ions from the back of the grain to the front. Furthermore, no new ordered structure can be seen near the interface between the crystal and amorphous regions. It indicates that the insertion of lithium ions destroys the crystal structure of Si directly instead of the formation of any intermediate phases.

With an increasing dose of inserted lithium ions, the amorphous regions develop further towards the

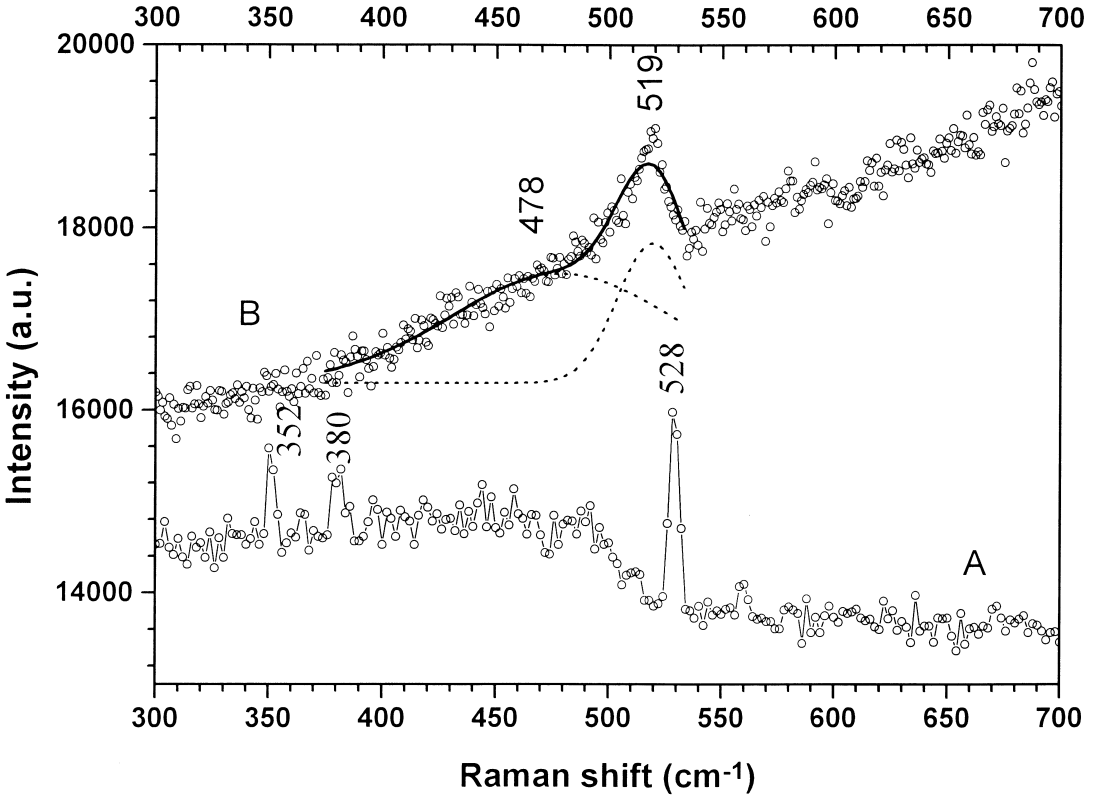

Fig. 4. Raman spectra of the Li-inserted SiNWs electrode after annealing treatment. (A) The same as that in Fig. 2(C); (B) after step (A), then vacuum-annealing at 400°C for 5 h.

core part of a SiNW as shown in Fig. 5(C), resulting in further shrinking of the crystalline regions. It could be observed that the original continuous crystalline region is divided into several slim stripes within the single SiNW. The dimension of these stripes is reduced to a few nanometers. As a result, the intensity of the photoluminescence spectra of Li-inserted SiNWs is increased significantly and the band of light emission is blue-shifted obviously [14].

At the more heavy insertion level ($>Li_{2.6}Si$), the ordered Si lattice in a SiNW could disappear completely as shown in Fig. 5(D), indicating a full transformation from crystalline SiNWs into amorphous Li–Si nanowires.

Fig. 5(E) shows the image of three SiNWs after lithium ions were partly extracted from the deeply inserted Li–Si nanowires. The crystalline regions denoted by white arrows can be seen clearly in the core part of SiNWs. The lattice spacing is about 0.31 nm. It indicates that the amorphous Li–Si nanowires recrystallize after extraction of part the lithium ions. It has been known before that random crystallization of pure amorphous silicon occurs above 600°C [22]. This indicates that the extraction of lithium ions promotes the nucleation and growth of Si in Li–Si nanowires.

The electrochemical extraction of lithium ions from SiNWs or SiNPs was performed by charging a discharged cell of SiNWs/Li or SiNPs/Li to 2.0 V and keeping the potentiostat at 2.0 V for 24 h. It was found that a larger irreversible capacity loss always exists [1]. According to the analysis on the discharge/charge curves of SiNPs/Li and SiNWs/Li cells, it is sure that the main part of the lost capacity is not caused by the decomposition reaction of the electrolyte. Based on the image of Fig. 5(E), Raman

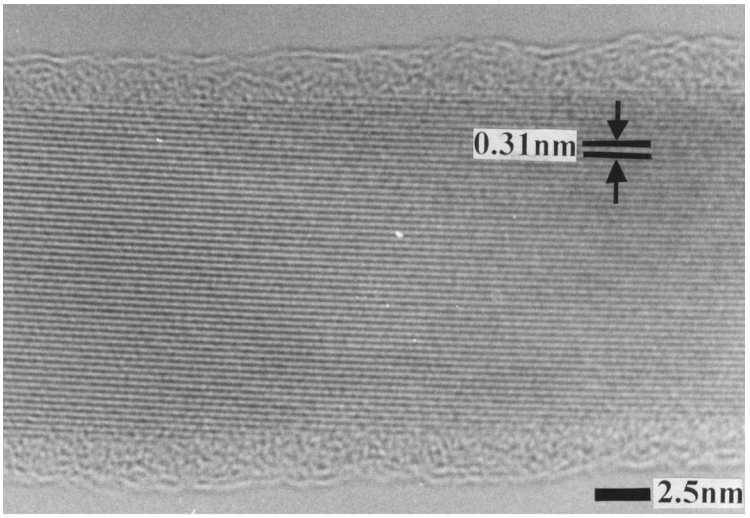

(A)

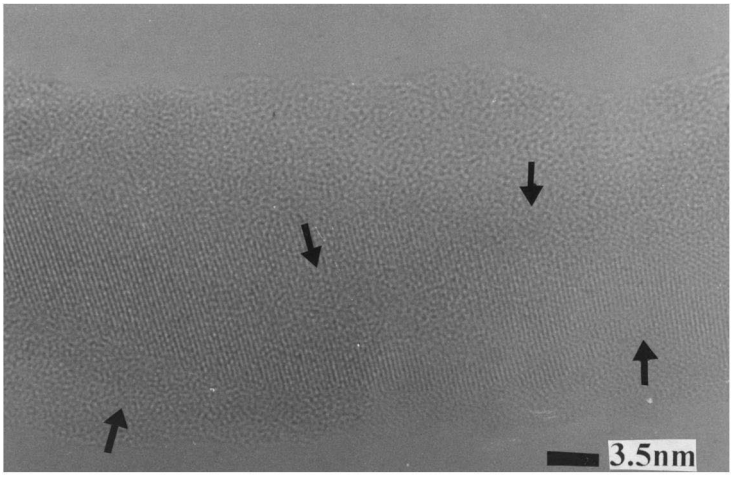

(B)

Fig. 5. The high resolution transmission electronic microscopy of SiNWs at different Li-insertion levels. (A) Original SiNWs, (B)–(E) after the same electrochemical treatment corresponding to Fig. 1(A)–(D), respectively.

spectra of Figs. 1(D) and 2(D), it can be concluded that the amorphous component still exists at the charged state. In fact, a large amount of intrinsic and insertion-generated defaults within the nanosized Si can produce a lot of dangling bonds. Those dangling bonds have a strong affinity to capture lithium ions. Wahl et al. has reported that substituted Li in Si can be kept stable at least up to 670 K [23]. Therefore, it may be very difficult to extract all the inserted lithium ions under current electrochemical conditions. The remaining lithium ions may modify the crystal structure of nanosized Si and act as the main resource of irreversible capacity loss.

It can also be noticed that two SiNW denoted by 1 and 2 in Fig. 5(E) have merged together. SiNW denoted by 3 seems to be hanging over SiNW 1. Recently, we have found that the aggregation of nanosized active particles caused by electrochemical

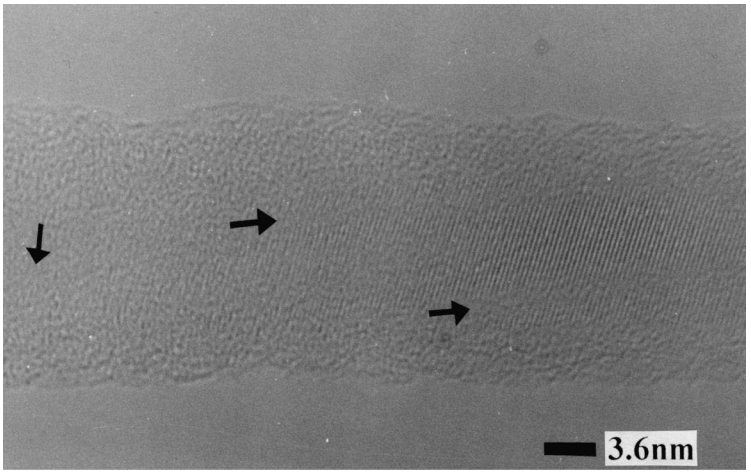

(C)

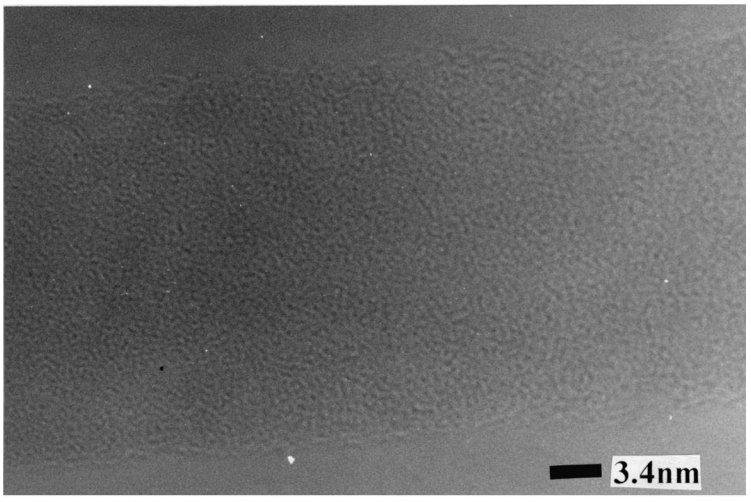

(D)

Fig. 5. (*continued*)

alloy reaction with lithium is a normal phenomenon [9,20,24]. It will be discussed in the following section.

Considering the result of Fig. 5, it can be deduced that the structure variation of nanosized Si from crystalline to amorphous and then back to crystalline is a reversible phase transformation. The influence of this variation on the electrochemical properties is not very clear. Since a better cyclic performance of SiNPs can be achieved by adding a large amount of carbon black [1], it seems that the effect of the transformation of the lattice structure could be ignored.

3.4. Morphology variation of SiNPs and SiNWs after Li-insertion

In fact, a large amount of merged SiNWs were observed at both the deep discharged state and charged state from the images of HRTEM [25]. The morphology variation of SiNPs caused by Li-insertion has also been investigated by SEM.

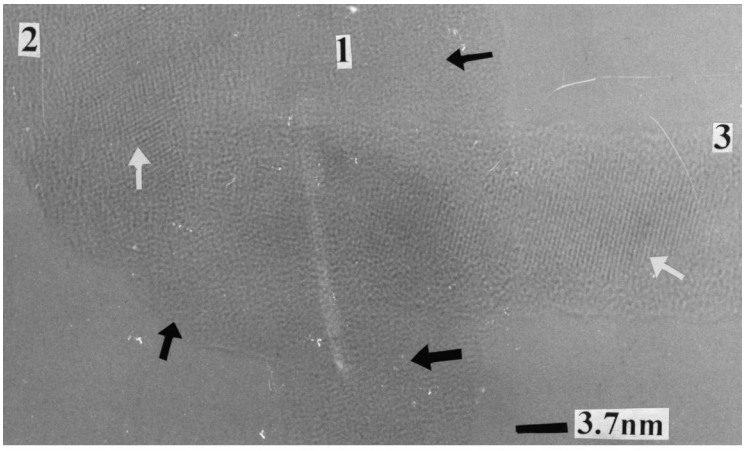

(E)

Fig. 5. (*continued*)

Fig. 6(A) shows an image of the original SINPs electrode in which the SiNPs powder was mixed with carbon black (CB) at a weight ratio of 1:1. The average particle size of the ball-shape CB is 40 nm [25]. It can be seen that SiNPs particles are interspersed among CB uniformly. However, when the SiNPs electrode was discharged to 0.0 V vs. Li/Li^+, an obvious agglomeration can be seen in Fig. 6(B). A continuous net structure with many cavities or holes was formed. From the zoom image as shown in Fig. 6(C), it can be seen more clearly that many dispersed particles coalesce into a strong flocculation structure. In view of the morphology variation, this phenomenon can be named as electrochemical sintering [26].

Fig. 6(D) and (E) show the images of the SiNPs electrode at a charged state after 20 cycles. The agglomeration is more significant. The number of cavities reduces further.

The morphology of the SiNPs electrode without CB at a charged state has been investigated by us [9]. A typical view of them is shown in Fig. 6(F). The separated SiNPs particles have agglomerated into very dense blocks denoted by a black arrow (the region denoted by a white arrow is the surface-rough Cu substrate). The width of each block is over several micrometers. Comparing Fig. 6(F) with Fig. 6(D) and (E), indicates that carbon black at this case does not restrain effectively the agglomeration of SiNPs particles. It is obvious that the dense structure is not propitious to the insertion and extraction of lithium ions in view of kinetics. In fact, although the reversible capacity still fades with cycle number, the cyclability of SiNPs adding with CB are much better than those without adding CB [1]. Therefore, it can be deduced that if serious agglomeration can be restrained effectively, the cyclic performance will be improved further. A recent study on a tin composite oxide (TCO) anode also confirmed that the oxide matrix can restrain the growth of nanosized Li–Sn alloys [19,20]. Thus, a suitable inert matrix is necessary to improve the electrochemical properties of nanosized alloy anodes.

It should be emphasized that this type of agglomeration force is very strong since each of the SiNWs and SiNPs is covered by a silicon oxide layer with a thickness of about 2 nm. A possible agglomeration mechanism is that the insertion of lithium ions expands the volume of each particle and increases the contact probability of separated particles. Due to the high surface energy of nanosized particles [27], it is beneficial to decrease the surface energy by merging. Especially when lithium ions bonded with surface Si atoms are extracted from the surface regions of SiNWs or SiNPs by the electrochemical method, those Si atoms of neighbor particles may have a strong affinity to bond together and form an agglomerated body.

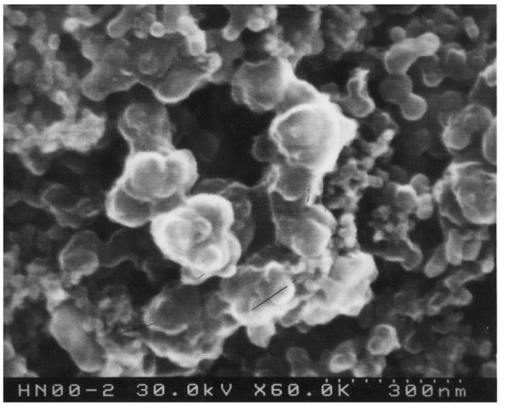

(A)

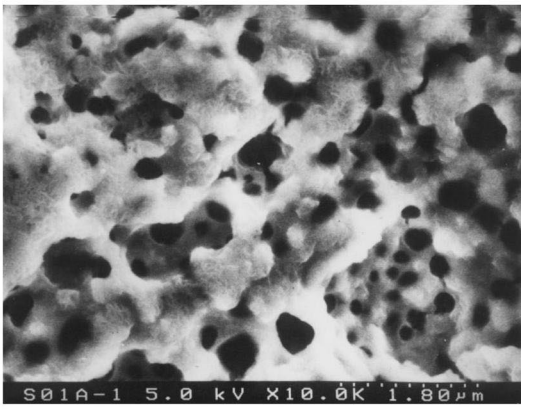

(B)

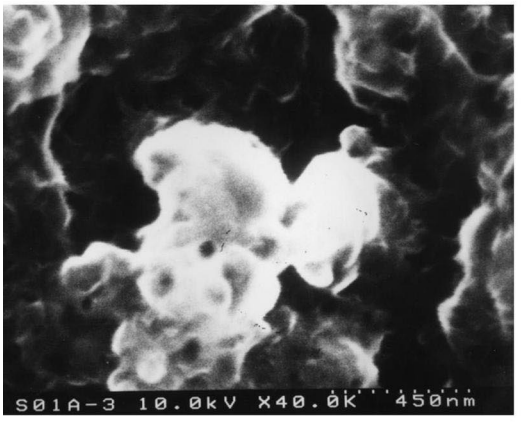

(C)

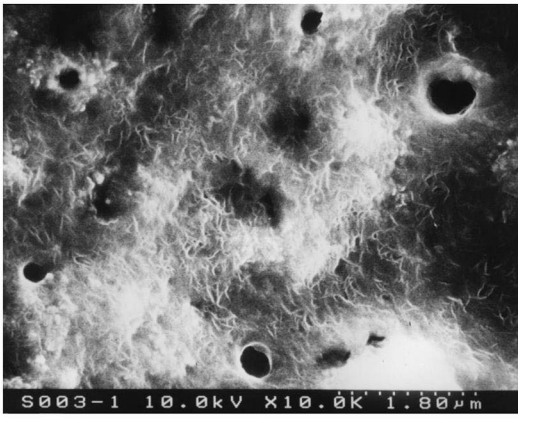

(D)

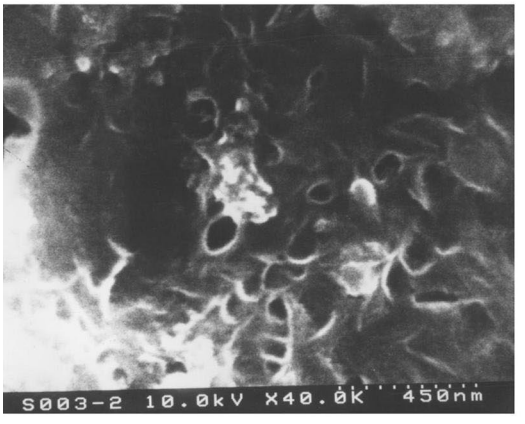

(E)

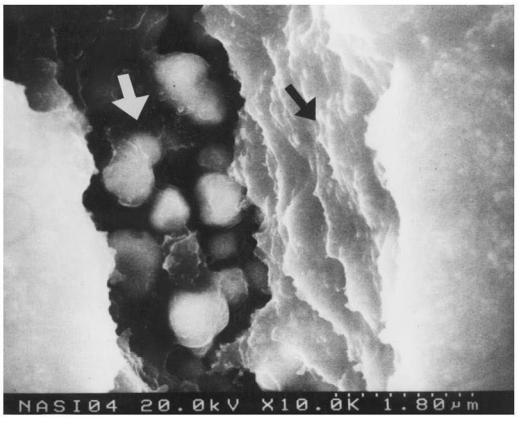

(F)

Fig. 6. The scanning electronic micrographs of the SiNPs electrode at different discharged states (A) original SiNPs electrode prepared by a mixture of SiNPs powder, carbon black and PVDF at a weight ratio of 4:4:2. (B) SiNPs electrode after the same electrochemical treatment as that described in Fig. 1(C). (C) Zoom part of Fig. 6(B). (D) SiNPs electrode after the same electrochemical treatment with Fig. 1(D). (E) Zoom part of Fig. 6(D). (F) A pure SiNPs electrode after the same electrochemical treatment with Fig. 1(D), the electrode was prepared in the same way as that described in the caption of Fig. 1.

4. Conclusions

The electrochemical insertion of lithium ions at room temperature destroys directly the crystal structure of Si leading to the formation of the metastable amorphous Li–Si alloy. After the extraction of partial lithium ions electrochemically, a local ordered structure can be obtained. The extraction of lithium ions promotes the recrystallization of amorphous Li-inserted Si at room temperature. This order–disorder transition is reversible. It is not easy to extract all inserted lithium ions from nanosized Si by the electrochemical method. Some lithium ions may be captured by unsaturated Si atoms resulting in the irreversible capacity loss. The nanosized Si particles have a strong tendency to merge together during the process of insertion/extraction of lithium ions.

Acknowledgements

This work was supported by Ford-NSFC Foundation (contact No. 9712304), NSFC (contact No. 59972041 and 19774022) and National 863 Key Program (contact No. 715-004-0280).

References

[1] H. Li, X.J. Huang, L.Q. Chen, Z.G. Wu, Y. Liang, Electrochem. Solid State Lett. 2 (1999) 547.
[2] S. Lai, J. Electrochem. Soc. 123 (1976) 1196.
[3] R.A. Sharma, R.N. Seefurth, J. Electrochem. Soc. 123 (1976) 1763.
[4] R.N. Seefurth, R.A. Sharma, J. Electrochem. Soc. 127 (1980) 1101.
[5] C.J. Wen, R.A. Huggins, J. Solid State Chem. 37 (1976) 271.
[6] R.N. Seefurth, R.A. Sharma, J. Electrochem. Soc. 124 (1977) 1207.
[7] B.A. Boukamp, G.C. Lesh, R.A. Huggins, J. Electrochem. Soc. 128 (1981) 725.
[8] K. Amezawa, N. Yamamoto, Y. Tomii, Y. Ito, J. Electrochem. Soc. 145 (1998) 1986.
[9] H. Li, X.J. Huang, L.Q. Chen, J.Q. Li, Y.Q. Zhou, Z.G. Wu, Y. Liang, (submitted).
[10] Y. Li, Y. Liang, K. Xiao, F. Zheng, Z. Hu, Acta Meta. Sinica 31 (1995) B21.
[11] D.P. Yu, C.S. Lee, I. Bello, X.S. Sun, Y.H. Tang, G.W. Zhou, Z.G. Bai, Z. Zhang, S.Q. Feng, Solid State Commun. 105 (1998) 403.
[12] A.M. Morales, C.M. Lieber, Science 279 (1998) 208.
[13] G.W. Zhou, Z. Zhang, Z.G. Bai, S.Q. Feng, D.P. Yu, Appl. Phys. Lett. 73 (1998) 677.
[14] H. Li, G.W. Zhou, D.P. Yu, X.J. Huang, L.Q. Chen, Z. Zhang, Appl. Phys. Lett. 75 (1999) 2447.
[15] Z. Iqbal, S. Veprek, J. Phys. C.: Solid State Phys. 15 (1982) 377.
[16] T. Motooka, O.W. Holland, Appl. Phys. Lett. 61 (1992) 3005.
[17] T. Motooka, O.W. Holland, Appl. Phys. Lett. 58 (1991) 2360.
[18] B.B. Li, D.P. Yu, S.L. Zhang, Phys. Rev. B 59 (1999) 1645.
[19] I.A. Courtney, J.R. Dahn, J. Electrochem. Soc. 144 (1996) 2045.
[20] H. Li, X.J. Huang, L.Q. Chen, Electrochem. Solid State Lett. 1 (1998) 241.
[21] H. Li, G.Y. Zhu, X.J. Huang, L.Q. Chen, J. Mater. Chem. 2000, in press.
[22] T.D. Chen, C.C. Koch, T.L. Mccormick, R.J. Nemanich, J.Y. Huang, J.G. Huang, J. Mater. Res. 10 (1995) 139.
[23] W. Wahl, H. Hofsaaa, S.G. Hahn, S. Winter, E. Recknagei, Appl. Phys. Lett. 62 (1993) 684.
[24] H. Li, L.H. Shi, W. Lu, X.J. Huang, L.Q. Chen (submitted).
[25] Hong Li, unpublished data.
[26] J.T. Vaughey, K.D. Keplar, D.R. Vissers, M.M. Thackeray, Abstracts of the 9th International Meeting on Lithium Batteries, Edinburgh, Scotland, July, 1998, Poster I, Tues 82.
[27] N. Ichinose, Y. Ozaki, S. Kashu (Eds.), Superfine Particle Technology, Springer–Verlag, London, 1992, p. 13.